Theory of diffusion-induced selective area growth of III-V nanostructures

Vladimir G. Dubrovskii*
Faculty of Physics, St. Petersburg State University, Universitetskaya Embankment 13B, 199034 St. Petersburg, Russia

(Received 2 November 2022; revised 22 January 2023; accepted 3 February 2023; published 14 February 2023)

Selective area growth of nanomembranes (NMs), nanofins, and planar nanowires (NWs) can pave the way for monolithic integration of III-V photonics with Si electronics and enable fabrication of scalable NW networks required for fundamental studies in low-temperature transport physics. Herein, we present an attempt to develop the kinetic growth theory of III-V NMs and related nanostructures in selective area epitaxy. The growth process is assumed to be driven by surface diffusion of group III adatoms. The populations of adatoms diffusing on the mask surface, NM sidewalls, and the top are described by three diffusion equations linked by six boundary conditions. The resulting growth equation provides the NM height as a function of time, slit width and pitch, and deposition conditions. The width and pitch dependences of the NM growth rate are found to be qualitatively different for different directions of the adatom diffusion fluxes (from the mask surface onto the NM or in the opposite direction). A good correlation of the model with the data on the growth kinetics of GaAs NMs by selective area molecular beam epitaxy is demonstrated.

DOI: 10.1103/PhysRevMaterials.7.026001

I. INTRODUCTION

Selective area growth (SAG) of III-V semiconductor materials on different masked substrates including Si, with lithographically defined openings in a mask layer, enables fabrication of regular arrays of nanomembranes (NMs), nanosheets, nanofins, planar nanowires (NWs), and advanced NW networks of different architectures [1–12]. Such structures have great potential in Si-integrated III-V photonics and high-speed electronics [2,3,8,10,11]. Scalable networks of III-V NWs and hybrid semiconductor-superconductor NW structures are required for fundamental studies of low-temperature transport physics, including test proposals for detection and manipulation with Majorana fermions [6,7,9]. SAG of complex III-V nanoheterostructures extends the mature technology of selective epitaxy of III-V materials [13,14] to the nanoscale. SAG consists of preparation of a mask (for example, SiO_2) on a semiconductor substrate (Si), lithographic patterning of the mask to fabricate the desired growth pattern, and deposition of a III-V material onto the patterned substrate [2]. Under the optimized conditions in terms of temperature and material fluxes, III-V growth occurs inside the openings but not on the mask surface [6]. Compared with other growth methods, such as the metal-assisted vapor-liquid-solid (VLS) growth of vertical NWs [15,16], SAG offers much wider opportunities for morphological design of one-dimensional (1D) or two-dimensional (2D) III-V nanostructures and their networks [2,6,7]. Planar 1D NWs and heterostructures based on 2D NMs achieved by SAG in 1D openings (slits) in a mask layer are more robust for processing, contacting, and device integration than heterostructures based on vertical NWs. In addition, the issue of unwanted Au contamination in Au-catalyzed VLS III-V NWs is safely avoided.

The achieved level of understanding and modeling of the SAG kinetics in 1D slits [2,6,7,17–20] is far below that established for VLS growth (see, for example, Ref. [21] for a review) or catalyst-free SAG [22–25] of vertical III-V NWs. The radius and pitch dependences of the axial growth rate of VLS III-V NWs have been studied in great detail vs the growth conditions in a given epitaxy technique and the corresponding mechanisms of material transport [21,26–35]. The width and pitch dependence of GaAs SAG in 1D slits has been addressed only recently [19]. This analysis led to some counterintuitive results. The GaAs growth rate was found to decrease with the pitch, while sparce arrays of slits are expected to collect more material per NM. This unusual behavior was explained by the inversion of Ga diffusion flux such that Ga adatoms diffuse from slit to mask rather than in the opposite direction. However, the semiqualitative diffusion model of Ref. [19] does not account for the height of NMs growing inside or outside the slit.

Consequently, in this paper, we make an attempt to develop a kinetic model for SAG of III-V nanostructures in patterned arrays of slits. According to the analysis of Ga-catalyzed VLS growth of GaP NWs on masked Si(111) substrates by molecular beam epitaxy (MBE) [26], there are two principally different mechanisms of material exchange between the mask surface and NWs: (i) surface diffusion of group III adatoms and (ii) re-emission of group III atoms from the mask. These two mechanisms lead to different vertical growth rates of VLS or SAG NWs [27,28]. The diffusion-induced character of GaAs SAG by MBE is confirmed by the results of Ref. [19]. Therefore, we assume that SAG of III-V materials is driven by surface diffusion, leaving re-emission for further study. The advanced theory of the diffusion-induced growth of VLS NWs treats group III adatoms on the substrate surface and NW

*dubrovskii.ioffe@mail.ru

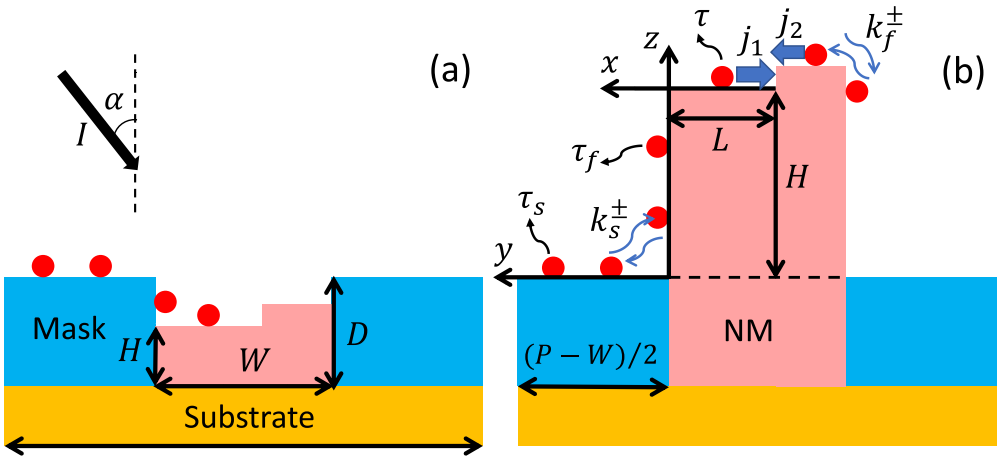

FIG. 1. Illustration of the model showing selective area growth (SAG) of rectangular nanomembrane (NM) with a constant width W (a) inside and (b) outside the slit in a mask layer.

sidewalls, with a metal alloy droplet resting at the NW top [33–35]. This requires two second-order diffusion equations for the surface and sidewall adatom subsystems. The corresponding boundary conditions include the pitch-dependent condition for zero flux between the NWs, a condition at the NW top which depends on the state of liquid droplet, and two conditions at the NW base containing the transition rates for the transfers of group III adatoms between the substrate surface and NW sidewalls [35]. Here, we consider three adatom subsystems diffusing on the mask surface, NM sidewalls, and top facet, which requires six boundary conditions and makes the whole treatment more difficult than for VLS NWs. The result explicitly provides the NM growth rate as a function of its width, pitch of 1D array of slits, group III flux, and kinetic constants such as transition rates and diffusion lengths of group III adatoms. Importantly, the governing equation is influenced by group V flux. Treatment of the initial stage of SAG inside the slit is based on the same equations as for large NMs. Overall, the developed approach allows for the detailed modeling and morphological control of NMs and related nanostructures in SAG approach, like what has been achieved for VLS NWs [21].

II. GROWTH MODEL

The model geometry of SAG inside and outside 1D slits is shown in Figs. 1(a) and 1(b), respectively. Although it is not critical, we consider SAG in the directional MBE technique, where the flux of group III atoms I ($\mathrm{nm^{-2}\,s^{-1}}$) is inclined by the angle α with respect to the substrate normal. Infinitely long slits having width W and depth D are separated by the pitch P. A rectangular III-V nanostructure having width W and height H_{tot} (including the part of the structure below the mask surface) is referred to as a NM, although it has 1D NW geometry for small enough H. It is assumed that the NM grows in the layer-by-layer mode, that is, the bottom of the slit is filled by III-V material from the very beginning. After that, the NM evolves only vertically (at a constant width W) by step flow on the flat top facet. This requires a stable facet parallel to the substrate plane to be energetically preferred and maintained during growth, as in the case of $\langle 111B\rangle$-oriented III-V NWs grown on Si(111) or GaAs(111)B substrates [22,24]. Geometries with nonplanar facets at the NM top can be described using the same model provided that the NM width W is constant during growth. In a more complex scenario, which occurs in SAG-MBE of GaAs NMs on GaAs(100) substrates [19], 3D NM does not fill the entire width of the slit in the initial growth stage. In this case, our model applies only to large enough NMs which have extended to the slit width. In the first approximation, we neglect possible polynuclear character of growth in the initial stage [19] if only one NM nucleates in each slit. We also ignore any extension of a NM above the width W if no III-V growth can occur on the mask. This is equivalent to the growth modeling of VLS NWs at a time-independent NW radius [29–31,33–35]. Usually, SAG-MBE of III-V nanostructures is performed under high V/III flux ratios. For example, the As/Ga flux ratio was 80 in Ref. [19]. In this case, SAG is limited by the kinetics of group III atoms, which is the usual assumption in modeling of Au-catalyzed VLS growth of III-V NWs [21,29–31,33–35].

We will first study the growth kinetics of large NM outside the slit, as shown in Fig. 1(b), and then demonstrate that the initial stage of SAG inside the slit [Fig. 1(a)] is described by the same equations with modified parameters. The NM height H is measured from the surface of the mask, that is, $H = H_{\mathrm{tot}} - D$. In the diffusion-induced growth, the net change in the NM volume is proportional to the total diffusion flux into the monolayer step propagating on the top facet $j = j_1 + j_2$, with j_1 and j_2 as the fluxes entering the NM from the two sides of the step of length L ($0 \leqslant L \leqslant W$). Three adatom subsystems diffusing on the mask surface (labeled s), NM sidewalls (labeled f), and top facet are described by the stationary diffusion equations [33,35]:

$$D_s\frac{d^2 n_s}{dy^2} + I\cos\alpha - \frac{n_s}{\tau_s} = 0,$$
$$D_f\frac{d^2 n_f}{dz^2} + I\sin\alpha - \frac{n_f}{\tau_f} = 0,$$
$$D\frac{d^2 n}{dx^2} + I\cos\alpha - \frac{n}{\tau} = 0. \qquad (1)$$

Here, D_s, D_f, and D are the diffusion coefficients of group III adatoms on the mask, NM sidewalls, and top, respectively, while τ_s, τ_s, and τ are the desorption-limited lifetimes of group III adatoms on these surfaces [see Fig. 1(b)]. The axes y, z, and x are chosen, as shown in Fig. 1(b), with $y = z = 0$ corresponding to the NM/mask edge and $x = 0$ to the monoatomic step at the NM top. Clearly, these equations require six boundary conditions.

By symmetry, the first boundary condition for n_s requires zero diffusion flux between the slits:

$$\left.\frac{dn_s}{dy}\right|_{y=(P-W)/2} = 0, \tag{2}$$

with $(P-W)/2$ being the distance from the NM/mask edge to the central band between the slits. For the two conditions at the transparent NM/mask edge, we use the reaction rate theory [36], employed previously in the NW [35] and NM [19] growth modeling:

$$D_s \left.\frac{dn_s}{dy}\right|_{y=0} = -D_f \left.\frac{dn_f}{dz}\right|_{z=0}, \tag{3}$$

$$-D_f \left.\frac{dn_f}{dz}\right|_{z=0} = k_s^+ n_s(y=0) - k_s^- n_f(z=0). \tag{4}$$

Equation (3) requires the continuity of diffusion flux at the NM/mask edge. According to Eq. (4), the diffusion flux through the transparent edge equals the difference between the number of adatom transfers from mask to NM and from NM to mask (per unit time and surface area). The k_s^+ and k_s^- (nm/s) denote the corresponding rate constants, as shown in Fig. 1(b). With these boundary conditions, the solution for n_f contains only one unknown constant B:

$$\begin{aligned} n_f =& I\tau_f \sin\alpha + B\cosh\left(\frac{z}{\lambda_f}\right) \\ &+ \left[\frac{\tau_f k_s^-}{\lambda_f \zeta} B - \frac{\tau_f (k_s^+ I\tau_s \cos\alpha - k_s^- I\tau_f \sin\alpha)}{\lambda_f \zeta}\right] \\ &\times \sinh\left(\frac{z}{\lambda_f}\right), \end{aligned} \tag{5}$$

with the pitch-dependent function:

$$\zeta = 1 + \frac{k_s^+ \tau_s}{\lambda_s} \mathrm{cotanh}\left(\frac{P-W}{2\lambda_s}\right). \tag{6}$$

Here, $\lambda_f = \sqrt{D_f \tau_f}$ and $\lambda_s = \sqrt{D_s \tau_s}$ are the desorption-limited diffusion lengths of group III adatoms on the mask surface and NM sidewalls, respectively.

A monoatomic step at the NM top is adsorbing rather than transparent. It can grow only when the chemical potential per III-V pair in the mother phase is higher than the equilibrium chemical potential. The latter is given by $k_B T \ln(n_3^{\mathrm{eq}} n_5^{\mathrm{eq}})$, where $n_3^{\mathrm{eq}} n_5^{\mathrm{eq}}$ is the temperature-dependent equilibrium activity per III-V pair in solid, T is the absolute temperature, and k_B is the Boltzmann constant [20]. We choose the boundary condition at the step edge in the form:

$$n(x=0) = \frac{n_3^{\mathrm{eq}} n_5^{\mathrm{eq}}}{n_5}, \tag{7}$$

with n_5 as a spatially uniform surface density of group V adatoms on the top facet. This condition ensured that the step grows at positive and dissolves at negative supersaturations of the 2D sea of group III and V adatoms. In the case of MBE, desorption of a group V element occurs in the form of dimers (such as As_2, P_2, or N_2) consisting of two group V adatoms which meet due to surface diffusion. Under group V-rich conditions where only a small fraction of group V atoms participate in stoichiometric growth, their incoming flux I_5 is equalized by desorption. Hence, $I_5 = 2D_5 n_5^2$, with D_5 as the effective diffusion coefficient of group V adatoms on the top NM facet. This gives

$$n_5 = \sqrt{I_5/2D_5}, \tag{8}$$

showing that the surface density of group V adatoms scales as $I_5^{1/2}$ [20]. The surface density of group III adatoms on the top facet is given by

$$n = I\tau\cos\alpha + C\sinh\left(\frac{x}{\lambda}\right) - \left(I\tau\cos\alpha - \frac{n_3^{\mathrm{eq}} n_5^{\mathrm{eq}}}{n_5}\right)\cosh\left(\frac{x}{\lambda}\right), \tag{9}$$

where $\lambda = \sqrt{D\tau}$ is the diffusion length on the top facet, and C is a constant. This solution applies to the part of the facet with $0 \leqslant x \leqslant L$, as shown in Fig. 1(b). These adatoms contribute into the diffusion flux j_1.

To find the unknown constants B and C, we use the boundary conditions at the upper NM edge of the form:

$$D\left.\frac{dn}{dx}\right|_{x=L} = -D_f \left.\frac{dn_f}{dz}\right|_{z=H}, \tag{10}$$

$$D\left.\frac{dn}{dx}\right|_{x=L} = k_f^+ n_f(z=H) - k_f^- n(x=L), \tag{11}$$

which are like Eqs. (3) and (4). The k_f^+ and k_f^- are the rate constants of the adatom transfers from the NM sidewall to the top and in the opposite direction. Using these conditions in Eqs. (5) and (9) yields the solutions for the three adatom surface densities n_s, n_f, and n. The diffusion flux j_1 is then obtained from

$$j_1 = D\left.\frac{dn}{dx}\right|_{x=0} = \frac{\lambda}{\tau} C. \tag{12}$$

The surface density of group III adatoms on the top facet is given by

$$\frac{n}{I\tau\cos\alpha} = 1 + \frac{j_1}{\lambda I\cos\alpha}\sinh\left(\frac{x}{\lambda}\right) - \Phi\cosh\left(\frac{x}{\lambda}\right).$$

The solution for the diffusion flux j_1 is obtained in the form:

$$j_1 = I\cos\alpha\left\{\lambda\Phi\tanh\left(\frac{L}{\lambda}+\psi\right) + \frac{1}{F[\cosh(L/\lambda)+\Gamma\sinh(L/\lambda)]}\left[l_f + \frac{k_f^+}{k_s^-}\frac{\gamma l_s}{\sinh(H/\lambda_f)+\gamma\cosh(H/\lambda_f)}\right]\right\}. \tag{13}$$

The parameter:

$$\Phi = 1 - \frac{n_3^{eq} n_5^{eq}}{n_5 I \tau \cos\alpha}, \tag{14}$$

is proportional to supersaturation of the 2D sea of group III and V adatoms on the top NM facet, with surface densities $I\tau\cos\alpha$ and n_5, respectively. Without surface diffusion of adatoms from NW sidewalls, a monoatomic step at the NM top can grow only when $\Phi > 0$. Therefore, Φ has the meaning of supersaturation of the vapor phase with respect to solid, which is drives the NM growth. The characteristic lengths l_f and l_s are given by

$$l_f = k_f^+ \tau_f \tan\alpha - k_f^- \tau, \quad l_s = k_s^+ \tau_s - k_s^- \tau_f \tan\alpha \tag{15}$$

and can be positive or negative depending on the transfer rates and desorption times on different surfaces. The parameter:

$$\gamma = \frac{\tau_f k_s^-}{\lambda_f \zeta}, \tag{16}$$

contains the pitch and width dependence through the combination $P-W$ in Eq. (6) for ζ. The functions ψ and F depend on H/λ_f according to

$$\psi = \operatorname{arctanh}(\Gamma), \tag{17}$$

$$\Gamma = \frac{\tau k_f^-}{\lambda F}, \quad F = 1 + \frac{k_f^+ \tau_f}{\lambda_f}\left[\frac{1 + \gamma \tanh(H/\lambda_f)}{\gamma + \tanh(H/\lambda_f)}\right]. \tag{18}$$

The solution for the diffusion flux j_2 is obtained following the same procedure, with the facet length L changed to $W-L$. Therefore, we have

$$j_2 = j_1(W - L). \tag{19}$$

The obtained solutions for the diffusion fluxes provide a detailed description of the SAG kinetics including the step flow on the NM top, whereby the facet length L changes from 0 to W. This stage is usually omitted in the transport equations describing the growth rates of VLS [30–35] or SAG [25,28] vertical NWs (we note that the monolayer growth in VLS III-V NWs is usually fast compared with the droplet refill [21] but can be influenced by the stopping effect due to depletion of group V atoms in the droplet [37]). To obtain a growth equation which neglects the fast progression of the step at the NM top, along with waiting time between the successive nucleation of steps, we use the averages of the diffusion fluxes over the NM width W. The coarse equation for the time evolution of the NM volume per unit length of the slit is then obtained from

$$\frac{dS}{dt} = W\frac{dH}{dt} = \Omega_{35}\frac{1}{W}\int_0^W dL[j_1(L) + j_2(L)]. \tag{20}$$

At a constant width W, this gives a growth equation describing the evolution of the NM height H (that is, the NM volume per unit area).

Averaging of the diffusion fluxes given by Eqs. (13) and (19) yields our main result:

$$\frac{dH}{dt} = 2\Omega_{35} I \cos\alpha \left\{ \frac{\lambda^2}{W^2}\Phi \ln\left[\frac{\cosh(W/\lambda + \psi)}{\cosh(\psi)}\right] + \frac{2\lambda}{W^2 F}\left[l_f + \frac{k_f^+}{k_s^-}\frac{\gamma l_s}{\sinh(H/\lambda_f) + \gamma\cosh(H/\lambda_f)}\right]\frac{1}{\sqrt{1-\Gamma^2}} \times \arctan\left[\frac{\sqrt{1-\Gamma^2}\tanh(W/2\lambda)}{1 + \Gamma\tanh(W/2\lambda)}\right]\right\}. \tag{21}$$

This kinetic equation describes three different contributions into the diffusion-induced SAG rate. The first, the Φ term gives the contribution of group III flux directly impinging the NM top and desorption of group III atoms from the top facet. This term is positive at $\Phi > 0$, corresponding to positive vapor supersaturation with respect to the top facet. The other two contributions are related to surface diffusion of group III adatoms. The second, the l_f term stands for group III adatoms diffusing from the NM sidewalls to the top (at $l_f > 0$) or in the opposite direction (at $l_f < 0$). The third, the l_s term describes group III adatoms diffusing from the mask surface onto the NM sidewalls (at $l_s > 0$) or in the opposite direction (at $l_s < 0$). This term cancels for high NMs with $H/\lambda_f \gg 1$, where the diffusion exchange between the mask surface and NM top facet becomes negligible. The deconvolution of different contributions into the total growth rate given by Eq. (21) is like VLS NWs, where the models of Refs. [32–35] considered the direct group III flux impinging the droplet, surface diffusion adatoms from the NW sidewalls, and substrate. Different directions of the diffusion fluxes (from the substrate and NW sidewalls into the droplet or in the opposite direction) and the related nonlinear effects in NW growth were studied in Ref. [33].

The initial stage of SAG within the slit, shown in Fig. 1(a), is described using the same procedure. The only difference is that the NM sidewalls are replaced with sidewalls of the slit in an oxide mask. Therefore, the resulting growth equation has the same form as Eq. (21) but with modified parameters:

$$\frac{dH}{dt} = 2\Omega_{35} I \cos\alpha \left\{ \frac{\lambda^2}{W^2}\Phi \ln\left[\frac{\cosh(W/\lambda + \tilde{\psi})}{\cosh(\tilde{\psi})}\right] + \frac{2\lambda}{W^2 \tilde{F}}\left[\tilde{l}_f + \frac{\tilde{k}_f^+}{\tilde{k}_s^-}\frac{\widetilde{\gamma l_s}}{\sinh[(D-H)/\tilde{\lambda}_f] + \gamma\cosh[(D-H)/\tilde{\lambda}_f]}\right] \times \frac{1}{\sqrt{1-\tilde{\Gamma}^2}}\arctan\left[\frac{\sqrt{1-\tilde{\Gamma}^2}\tanh(W/2\lambda)}{1 + \tilde{\Gamma}\tanh(W/2\lambda)}\right]\right\}. \tag{22}$$

Here, the diffusion length $\tilde{\lambda}_f$ corresponds to the sidewall of the slit. The modified characteristic lengths $\tilde{l}_f$ and $\tilde{l}_s$ are given by

$$\tilde{l}_f = \tilde{k}_f^+ \tilde{\tau}_f \tan\alpha - \tilde{k}_f^- \tau, \quad \tilde{l}_s = \tilde{k}_s^+ \tau_s - \tilde{k}_s^- \tilde{\tau}_f \tan\alpha. \tag{23}$$

The $\tilde{k}_f^{\pm}$ denote the rate constants for the transfer of group III adatoms from the sidewalls of the slit to the NM top facet and in the opposite direction. The $\tilde{k}_s^{\pm}$ are the rate constant for the transfer of group III adatoms from the mask surface to the sidewalls of the slit and in the opposite direction. Other parameters are modified to

$$\tilde{\gamma} = \frac{\tilde{\tau}_f \tilde{k}_s^-}{\tilde{\lambda}_f \tilde{\zeta}}, \quad \tilde{\zeta} = 1 + \frac{\tilde{k}_s^+ \tau_s}{\lambda_s} \text{cotanh}\left(\frac{P-W}{2\lambda_s}\right), \tag{24}$$

$$\tilde{\psi} = \text{arctanh}(\tilde{\Gamma}), \tag{25}$$

and

$$\tilde{\Gamma} = \frac{\tau \tilde{k}_f^-}{\lambda \tilde{F}}, \quad \tilde{F} = 1 + \frac{\tilde{k}_f^+ \tilde{\tau}_f}{\tilde{\lambda}_f}\left[\frac{1+\gamma \tanh[(D-H)/\tilde{\lambda}_f]}{\gamma + \tanh[(D-H)/\tilde{\lambda}_f]}\right]. \tag{26}$$

In the expression for $\tilde{F}$, the height of slit sidewalls equals $D-H$. These equations apply to the initial stage which continues before the NM height reaches the slit depth D.

In the limiting case of high surface diffusivity on the NM top ($W/\lambda \ll 1$and $\tau k_f^-/\lambda \ll 1$), the growth equation given by Eq. (22) is reduced to

$$\frac{dH}{dt} = \Omega_{35} I \cos\alpha \left\{\Phi + \frac{2}{WF}\left[L_f + \frac{L_s}{\sinh(H/\lambda_f)/\gamma + \cosh(H/\lambda_f)}\right]\right\}, \tag{27}$$

with the characteristic lengths:

$$L_f = k_f^+ \tau_f \tan\alpha - k_f^- \frac{n_3^{\text{eq}} n_5^{\text{eq}}}{n_5 I \cos\alpha}, \quad L_s = \frac{k_f^+}{k_s^-}(k_s^+ \tau_s - k_s^- \tau_f \tan\alpha). \tag{28}$$

For short enough NMs with $H/\lambda_f \ll 1$, this is further simplified to

$$\frac{dH}{dt} = \Omega_{35} I \cos\alpha \left(\Phi + \frac{2L_*}{WF}\right),$$
$$L_* = L_f + L_s = k_f^+ \frac{k_s^+}{k_s^-}\tau_s - k_f^- \frac{n_3^{\text{eq}} n_5^{\text{eq}}}{n_5 I \cos\alpha}, \tag{29}$$

with the pitch-dependent F given by

$$F = 1 + \frac{k_f^+}{k_s^-}\zeta. \tag{30}$$

Equations (27) and (29) have a clear physical meaning. In the initial growth stage where desorption of group III adatoms from the short NM sidewalls is negligible, the NM height increases due to direct impingement of group III atoms without a desorbed fraction, collection of group III atoms from length L_f on the NM sidewalls and length L_s on the mask surface, as given by Eq. (29) with the effective collection length $L_* = L_f + L_s$. The factor F in Eqs. (27) and (29) accounts for the pitch dependence of SAG rate and rate constants for the adatom transfers between different surfaces. Without surface diffusion ($L_* = 0$) and desorption ($\Phi = 1$), the NM height evolves at the MBE deposition rate, which equals the 2D equivalent growth rate

$$v = \Omega_{35} I \cos\alpha. \tag{31}$$

The fraction of adatoms desorbed from the NM sidewalls before reaching the top gradually increases with the NM height. Finally, no surface adatoms can reach the NM top, and only the sidewall collection remains, yielding the growth equation for high NMs of the form:

$$\frac{dH}{dt} = \Omega_{35} I \cos\alpha \left(\Phi + \frac{2L_f}{WF}\right), \quad H/\lambda_f \gg 1, \tag{32}$$

with

$$F = 1 + \frac{k_f^+ \tau_f}{\lambda_f}. \tag{33}$$

This F is independent of pitch because the contribution of group III adatoms diffusing on the mask surface becomes negligible. Therefore, high enough NM grows due to direct impingement and collection of group III atoms from the upper part of the NM of length L_f.

According to Eq. (28), the characteristic length L_f is positive when the number of direct transfers adatoms from the NM sidewalls (with the desorption-limited lifetime τ_f) to its top is larger than the number of reverse adatom transfers from the NM top to its sidewalls, and negative otherwise. The characteristic lifetime of adatoms on the NM top equals $n_3^{\text{eq}} n_5^{\text{eq}}/(n_5 I \cos\alpha)$ and decreases with I and n_5 [or with I_5 according to Eq. (8)]. The characteristic length L_s is positive when the number of direct transfers of adatoms from the mask surface (with the desorption-limited lifetime τ_s) to the NW sidewalls is larger than the number of reverse adatom transfers from the NM sidewalls to the mask. In Ref. [19], it was argued that the desorption from an inert mask should be much faster than from a semiconductor surface such as the NM sidewall facet, which is why $\tau_s \ll \tau_f$. From Eq. (28), this may yield large negative L_s even at $k_s^+ > k_s^-$. The number of reverse adatom transfers in L_f can easily be decreased by increasing both group III and V fluxes, while the L_s value is flux independent. Unfortunately, very little is known about the rate constants $k_s^{\pm}$ and $k_f^{\pm}$ and their temperature dependence. It is well known, however, that temperature dependence of the desorption-limited lifetimes τ_s, τ_f, and τ has the Arrhenius form with high activation energies of the order of several electronvolts [6,20]. It is expected that τ_s decreases with temperature much faster than τ_f, which makes negative L_s and L_* in Eqs. (27) and (29) even more probable in the high-temperature range. On the other hand, high temperatures are often required to suppress parasitic nucleation on the mask surface to ensure the growth selectivity [6,19,20].

Based on these considerations and the results of Ref. [19], which clearly reveal that Ga adatoms diffuse from the slit onto the mask surface in the initial stage of GaAs SAG, the growth at $\Phi > 0$, $L_f > 0$, and $L_* < 0$ is very likely. Considering the simplified case of $\tilde{k}_s^{\pm} = k_s^{\pm}$, $\tilde{k}_f^{\pm} = k_f^{\pm}$, and $\tilde{\lambda}_f = \lambda_f$, the NW growth kinetics are identical inside and outside the slit, and the growth laws given by Eqs. (21), (27), and (29) apply for any H starting from the bottom of the slit. In this scenario, Eq. (29) shows that NMs of any width can emerge at $L_* > 0$. At

$L_* < 0$, NMs can still emerge due to positive Φ provided that their width is larger than the critical width $W_c = 2|L_*|/(F\Phi)$. Thinner NMs cannot be grown at $L_* < 0$.

This effect is related to the shape of adatom concentration profiles on the top facet. For small enough structures with $W/\lambda \ll 1$, the diffusion fluxes given by Eqs. (13) and (19) are reduced to

$$j_1 = j_2 = j = I\cos\alpha\left(\frac{W\Phi}{2} + \frac{L_*}{F}\right). \tag{34}$$

The adatom densities on the top facet are given by

$$\frac{n}{I\tau\cos\alpha} = 1 - \Phi\cosh\left(\frac{x}{\lambda}\right) + \frac{1}{\lambda}\left(\frac{W\Phi}{2} + \frac{L_*}{F}\right)\sinh\left(\frac{x}{\lambda}\right),$$
$$\frac{n'}{I\tau\cos\alpha} = 1 - \Phi\cosh\left(\frac{W-x}{\lambda}\right) + \frac{1}{\lambda}\left(\frac{W\Phi}{2} + \frac{L_*}{F}\right) \times \sinh\left(\frac{W-x}{\lambda}\right), \tag{35}$$

where $n(x)$ and $n'(x)$ describe the concentration profiles on the left ($0 \leqslant x \leqslant L$) and right ($L \leqslant x \leqslant W$) sides of the step. At $L_* > 0$, adatom concentration decreases toward the step, corresponding to positive diffusion flux of group III adatoms starting from the NM sidewalls. At $L_* < 0$, the derivative dn/dx becomes zero at the distance x_* given by

$$\tanh\left(\frac{x_*}{\lambda}\right) = \frac{1}{\lambda}\left(\frac{W}{2} - \frac{|L_*|}{F\Phi}\right), \quad x_* \cong \frac{W}{2} - \frac{|L_*|}{F\Phi}, \tag{36}$$

where the approximate λ-independent solution corresponds to $W/\lambda \to 0$. Therefore, group III atoms are collected only from the inner part of the top facet where $dn/dx > 0$. Atoms impinging on the outer part of the top facet with $dn/dx < 0$ leave the facet and diffuse through the NM edge along the sidewalls to the mask surface and ultimately desorb from the mask. For very thin NMs with $W \leqslant W_c$, all group III adatoms diffuse onto the mask surface, which is why such NMs cannot grow even at positive Φ. This behavior is illustrated in Fig. 2.

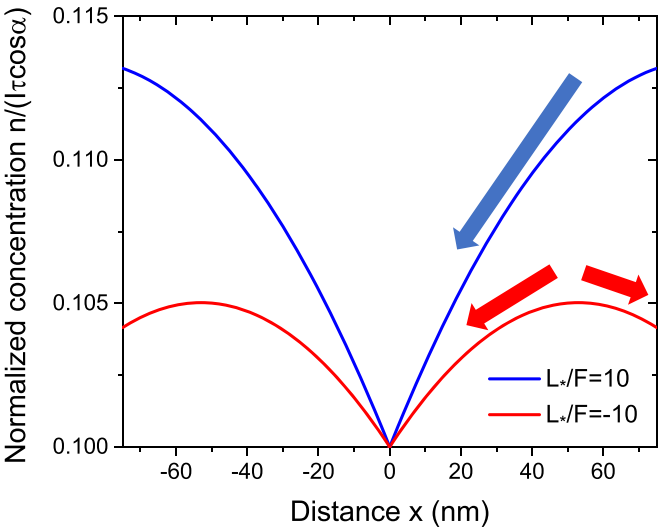

FIG. 2. Adatom concentration profiles on the top facet, obtained from Eq. (31) with $L = W/2$ at a fixed $W = 150$ nm, $\Phi = 0.9$, $\lambda = 500$ nm, and two different $L_*/F = 10$ and -20. Arrows indicate the directions of diffusion fluxes. The diffusion flux through the nanomembrane (NM) edge is positive for positive L_* and negative otherwise.

III. RESULTS AND DISCUSSION

Let us first analyze the pitch and width dependence of the NM growth rates. From Eqs. (29) and (30) describing the initial growth stage, the pitch dependence is present only in the function ζ given by Eq. (6). The width dependence is present in ζ and in the $1/W$ factor of the diffusion-induced growth rate. The NM growth rate increases with P and decreases with W at $L_* > 0$. When the diffusion flux of group III adatoms is directed from the mask surface into the slit or onto the NM sidewalls, sparce and thinner NMs grow faster than dense and thick NMs. This tendency is like vertical VLS NWs growing by surface diffusion of adatoms, where thinner NWs grow faster due to a larger diffusion flux into the droplet [28–35] and sparce NWs grow faster because more group III atoms per NW are collected by the substrate surface [35,38,39]. The situation is reversed at $L_* < 0$. In this case, the diffusion flux takes away a fraction of group III atoms which would otherwise contribute to the NM growth. The NM growth rate decreases with P and increases with W because less group III adatoms are lost for growth of denser and thicker arrays of NMs. High enough NMs receive no adatom flux from the mask surface. Hence, their growth rate is independent of pitch, as given by Eqs. (32) and (33). As for the width dependence, the growth rate of high NMs decreases with W at $L_f > 0$, as in the diffusion-induced growth of long enough VLS NWs [28–35].

Figure 3 shows the pitch-dependent NM growth rates, obtained from Eq. (26) at a fixed NM width of 100 nm, $\Phi = 0.5$, $\lambda_s = 500$ nm, $L_f = 100$ nm, and two different L_s of 50 nm (corresponding to positive diffusion flux from the mask surface onto the NM at $L_* = 50$ nm) and -150 nm (corresponding to negative diffusion flux from the NM onto the mask surface at $L_* = -100$ nm). As discussed, the growth rates increase with P in Fig. 3(a) and decrease with P in Fig. 3(b). At $\lambda_s = 500$ nm, the growth rates become insensitive to pitch >2000 nm, so that the curves at $P = 2000$ and 4000 nm are almost indistinguishable in both figures. In the initial growth stage corresponding to small $H/\lambda_f \ll 1$, the NM growth rates are much smaller than deposition rate v for negative diffusion flux from NM to mask and larger than v for positive flux from mask to NM. For very high NMs with $H/\lambda_f \ll 1$, all curves in Figs. 3(a) and 3(b) converge to the same asymptotic growth rate corresponding to a fixed Φ and L_f, as given by the pitch-independent Eqs. (32) and (33).

Figure 4 shows the width-dependent NM growth rates, obtained from Eq. (26) with the same parameters as in Fig. 3 at a fixed pitch of 1000 nm. At $L_s = 50$ nm, the growth rates decrease with width for any H/λ_f [Fig. 4(a)]. The situation at $L_s = -150$ nm is more complex. At the beginning of growth, thicker NMs grow faster. The increasing width dependence converges to the decreasing one at $H/\lambda_f \cong 0.25$, meaning that thinner NMs start to grow faster due to $L_f > 0$ in a later stage. The width of 50 nm is below the critical width for these parameters, which is why the growth rate of

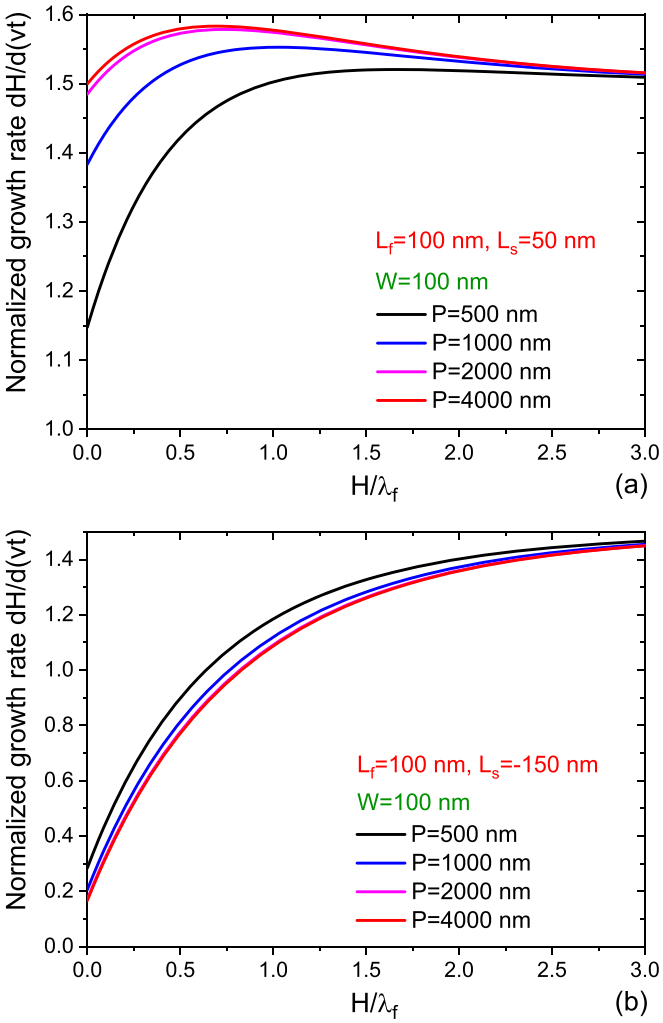

FIG. 3. Pitch-dependent vertical growth rates of nanomembranes (NMs) vs dimensionless height H/λ_f, obtained from Eq. (27) at a fixed width W of 100 nm, $\Phi = 0.5$, $\lambda_s = 500$ nm, $L_f = 100$ nm, for (a) positive ($L_s = 50$ nm) and (b) negative ($L_s = -150$ nm) diffusion fluxes from the mask surface into the slit and onto the NM sidewalls. The growth rates increase with pitch in (a) and decrease in (b). In both cases, the pitch dependence saturates for large P so that the curves at $P = 2000$ and 4000 nm are almost indistinguishable. The growth rates in (a) are much large than in (b) for small enough H/λ_f corresponding to the initial growth stage of short NMs. However, both growth rates converge to the same pitch-independent asymptote at large $H/\lambda_f \gg 1$.

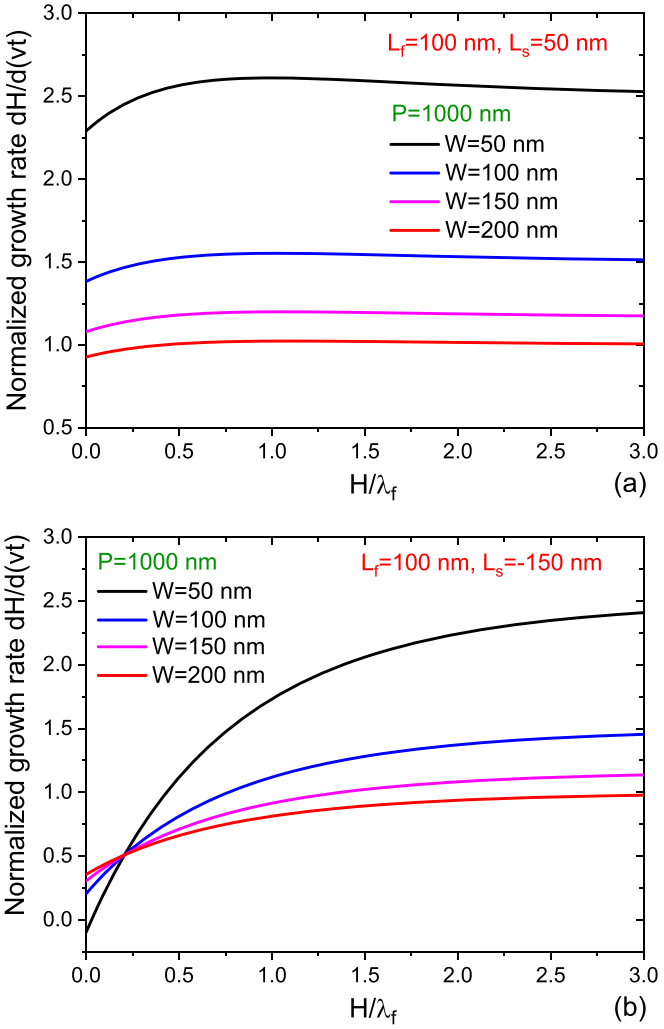

FIG. 4. Same as Fig. 3 for the width-dependent growth rates. The curves are obtained from Eq. (27) for the same parameters as in Fig. 3, at a fixed pitch P of 1000 nm. The growth rates decrease with width for positive diffusion flux shown in (a), that is, thinner nanomembranes (NMs) grow faster. For negative diffusion flux shown in (b), the width dependence converges at around $H/\lambda_f = 0.25$, meaning that short NMs grow faster for larger width, while tall NMs grow faster for smaller width. At $W = 50$ nm, the growth rate is negative for very small H/λ_f, meaning that such thin NMs cannot emerge without changing the growth conditions. At a given width, the growth rates in (a) and (b) converge to the same asymptote at large $H/\lambda_f \gg 1$.

50 nm NM is negative at $H/\lambda_f \to 0$. Such a thin NM can only continue growing starting from a certain height but cannot be nucleated on the bottom of the slit without changing the growth conditions (for example, temperature or material fluxes).

The two limiting behaviors of the NM growth kinetic are given by the height-independent growth rates given by Eq. (29) at $H/\lambda_f \ll 1$ and Eq. (32) at $H/\lambda_f \gg 1$. Therefore, the height of very shorth and very tall NMs is linear in time. No exponential growth stage is present in the NM growth kinetics, while it is often observed for VLS NWs [32–35,38,40]. To understand the NM height evolution at any time, we consider the simplified case of Eq. (27) at $\gamma = 1$. Such growth can be observed, for example, when $(P-W)/2\lambda_s \gg 1$, with $\zeta = 1 + k_s^+\tau_s/\lambda_s = \text{const.}$ according to Eq. (6), $\gamma = \tau_f k_s^-/(\lambda_f \zeta) = 1$, and $F = 1 + k_f^+/k_s^- = \text{const.}$ as given by Eq. (30) at $\gamma = 1$. Integration of Eq. (27) at $\gamma = 1$ gives

$$H = \lambda_f \ln\left[\left(1 + \frac{b}{\Phi + a}\right)e^{(\Phi+a)vt/\lambda_f} - \frac{b}{\Phi + a}\right], \tag{37}$$

with

$$a = \frac{L_f}{WF}, \quad b = \frac{L_s}{WF}. \tag{38}$$

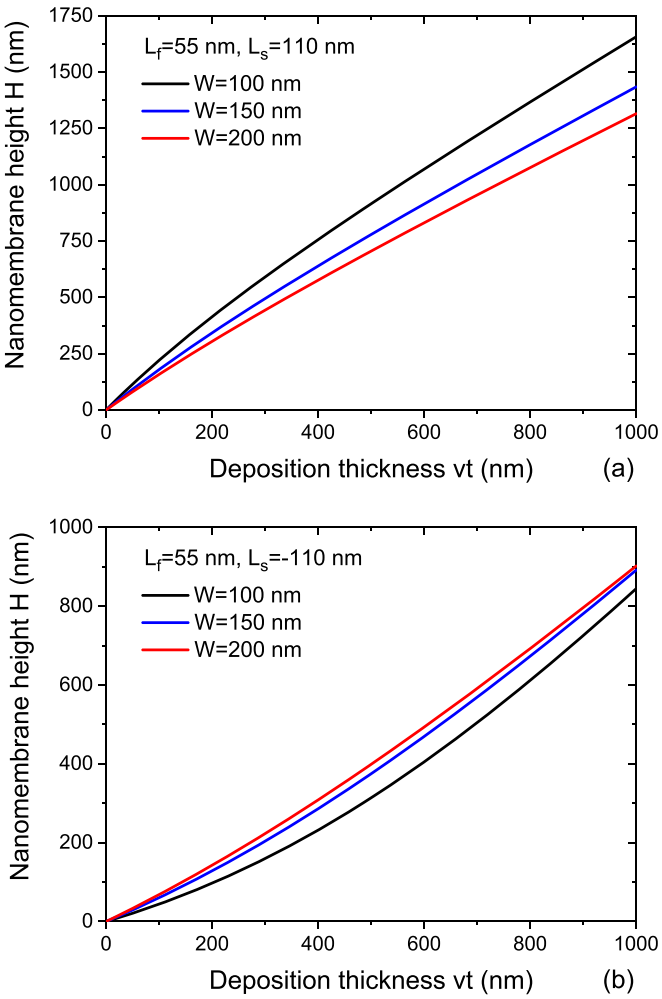

FIG. 5. Nanomembrane (NM) height vs deposition thickness, obtained from Eqs. (37) and (38) at a fixed Φ of 0.9, $\lambda_f = 500$ nm, $L_f = 55$ nm, and $F = 1.1$ at (a) positive ($L_s = 110$ nm) and (b) negative ($L_s = -110$ nm) diffusion fluxes from the mask surface into the slit and onto the NM sidewalls, for three different widths shown in the legend. The $H(vt)$ dependences are sublinear in (a) and superlinear in (b), although the NMs are systematically higher in (a). Thinner NMs grow faster in (a) and slower in (b).

For short growth times, this is reduced to the linear growth law $H = (\Phi + a + b)vt$. In the large time interpolation, the growth law is again linear, $H = \text{const.} + (\Phi + a)vt$, but the NM growth rate is different. Assuming $L_f > 0$ or $a > 0$, short NMs grow faster than taller ones at $L_s > 0$ or $b > 0$. In this case, the NM height evolution is sublinear in time. Conversely, at $L_s < 0$ or $b < 0$, the NM growth rate increases with time. Short NMs grow slower than taller ones, leading to superlinear NM height evolution. These properties remain in the general case with $\gamma \neq 1$ in Eq. (27).

Figure 5 shows the NM height vs the effective deposition thickness vt at a fixed Φ of 0.9, $\lambda_f = 500$ nm, $L_f = 55$ nm, and $F = 1.1$ for positive [$L_s = 110$ nm, Fig. 5(a)] and negative [$L_s = -110$ nm, Fig. 5(b)] diffusion fluxes from the mask surface onto the NM. The curves are sublinear in Fig. 5(a) and superlinear in Fig. 5(b) for any NM width W, although the NMs are higher in Fig. 5(a). The NM growth is faster in thinner slits for positive diffusion flux in Fig. 5(a), while it is slower in thinner slits for negative diffusion flux in Fig. 5(b).

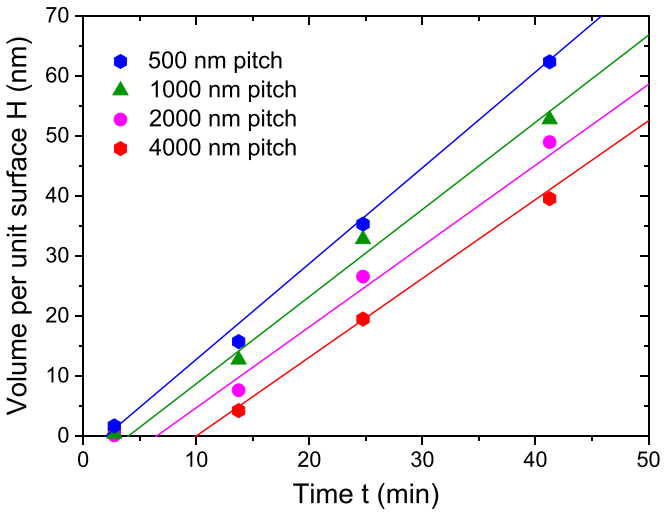

FIG. 6. Height of GaAs nanomembranes (NMs) vs time at a fixed width of 160 nm and different pitches shown in the legend (symbols) [19], fitted by Eqs. (29), (30), and (6) with the parameters described in the text (lines). In all cases, the evolution of NMs is linear in time.

We now consider the data of Ref. [19], where GaAs NMs were grown by MBE on GaAs(100) substrates covered with a 25-nm-thick SiO_2 mask. Slits of different widths and pitches were extended along the $01\bar{1}$ direction. GaAs deposition was performed with a Ga-limited 2D equivalent growth rate v of 1.8 nm/min, at a temperature of 630 °C and a V/III flux ratio of 80, which ensured the growth selectivity under As-rich conditions, for different times from 2 to 55 min. The GaAs NM growth on GaAs(100) substrates had three-dimensional (3D) character from the very beginning. More precisely, the $01\bar{1}$-oriented NMs nucleated as 3D islands restricted by the (311) side facets, which transitioned to (111) side facets after NMs extended to the slit width W. Figure 6 shows the measured height (that is, volume per unit surface area) of GaAs NMs grown in 160-nm-wide slits with different pitches P from 500 to 4000 nm. The NMs nucleated after an incubation time which was longer for larger P. According to Fig. 6, the NM heights evolved linearly with time for any P. NMs grown in slits with larger pitches were systematically shorter. This behavior was explained by negative diffusion flux of Ga adatoms from slits to mask [19]. Our growth model generalizes the approach of Ref. [19] by considering the NM geometry inside or outside the slit and three different populations of adatoms on the mask surface, slit or NM sidewalls, and NM top. Equation (29) at $H/\lambda_f \ll 1$ is directly applicable because the maximum NM height in Fig. 6 does not exceed 70 nm.

The lines in Fig. 6 show the linear fits to the data obtained from Eqs. (29), (30), and (6) with $v = 1.8$ nm/min, $\Phi = 0.99$, $W = 160$ nm, $L_* = -45$ nm, $\lambda_s = 750$ nm, $k_f^+/k_s^- = 1.2$, and $k_f^+ k_s^+ \tau_s/(k_s^- \lambda_s) = 0.95$. The incubation times obtained from linear fits to the data equal 2, 4, 6.5, and 10 min for 500, 1000, 2000, and 4000 nm pitch, respectively. Increasing the pitch of slit array results in the simultaneous decrease of the incubation time for NM growth and the slope angle of the linear time dependence of NM height. As discussed above, the

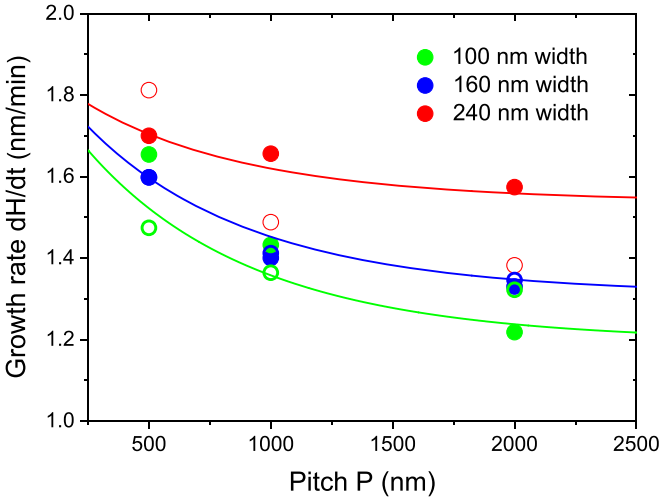

FIG. 7. Summary of the experimental growth rates of GaAs nanomembranes (NMs) for different pitches and widths (filled symbols) [19], modeling results of Ref. [19] (open symbols), and fits by Eqs. (29), (30), and (6) (lines).

increase of the NM growth rate with pitch necessarily requires negative diffusion flux of Ga adatoms from NMs to mask, corresponding to a negative L_* of -45 nm. In this respect, our model explains the effect in the same way as the model of Ref. [19]. However, quantitative results are different. This is demonstrated in Fig. 7, which summarizes the measured growth rates of GaAs NMs for different pitches and widths. The open symbols show the modeling results of Ref. [19], which converge to the same width-independent asymptote for pitches >2000 nm. Equation (29) contains the $1/W$ width dependence which remains even at $(P-W)/2\lambda_s \gg 1$. Consequently, the pitch-independent asymptotes of the growth rates are different for different widths and describe the observed increase of the growth rates with width much better than the 2D model of Ref. [19].

IV. CONCLUSIONS

In conclusion, the developed model provides a detailed description of diffusion-induced SAG of different III-V nanostructures including NMs and planar NWs. Treatment of three adatom subsystems diffusing on the mask surface, NM sidewalls, and top facet with the appropriate boundary conditions for the corresponding diffusion equations results in the growth equation which includes the fast kinetics of the monolayer progression on the top facet. Averaging this equation over the monolayer growth cycle yields the coarse equation containing the contributions from the direct impingement, diffusion on the mask surface and NM sidewalls. It has been shown that the NM growth rate decreases with its width and increases with pitch for positive diffusion of adatoms from the mask surface onto the NMs and features the opposite behavior when the diffusion flux is reversed. The time dependence of the NM height is given by the two linear dependences with different slope angles for short and tall NMs, connected by a nonlinear section whose shape depends on the direction of the adatom diffusion flux. The model provides good fit to the data on the growth kinetics of GaAs NMs by SAG-MBE on patterned SiO_2/GaAs(100) substrates. The developed approach is not specific for MBE and can be extended for modeling SAG in different vapor deposition techniques including metal organic vapor phase epitaxy. This will require additional considerations of the attachment-detachment kinetics and vapor composition influencing the supersaturation values relative to different surfaces. Furthermore, the model can be applied to other material systems such as III-nitrides, elemental semiconductors Si and Ge, II-VI compound semiconductors, and oxides.

These results provide a basis for modeling and controlling SAG in a wide range of epitaxy techniques, material systems, and template geometries. However, the model requires further development in several directions. First, the very beginning of SAG in the slits needs to be considered in more detail, including possible polynuclear growth of 3D structures and their coalescence [19]. Second, we assumed the flat top facet of a NM, as in the case of GaAs NMs growing perpendicular to (111)-oriented substrates. A more complex analysis should include 3D effects related to surface energy anisotropy, orientation-dependent growth kinetics on different surfaces, and possible shape transformations of a NM, such as reported in Ref. [17] for homoepitaxial GaAs nanofins. Strain-induced effects for heteroepitaxy of GaAs and other III-V NMs on lattice-mismatched Si substrates should be studied separately. Third, the shadowing effect in the directional MBE technique [26–28] and its possible impact on the growth kinetics should be considered. This is particularly important for SAG with large diffusion lengths of group III adatoms. Fourth, possible extension of NMs in the direction parallel to the substrate plane should be included, like the radial growth of vertical NWs [23,24,26,27,32]. Finally, re-emission of group III atoms from the mask surface [26,27] needs to be considered as the alternative mechanism of the material exchange between the mask surface and NM array. We plan to implement these modifications in the forthcoming work.

ACKNOWLEDGMENT

The author gratefully acknowledges financial support of the research grant of St. Petersburg State University (Grant No. ID 94033852).

[1] J. A. Rogers, M. G. Lagally, and R. G. Nuzzo, Synthesis, assembly and applications of semiconductor nanomembranes, Nature (London) **477**, 45 (2011).

[2] X. Yuan, D. Pan, Y. Zhou, X. Zhang, K. Peng, B. Zhao, M. Deng, J. He, J. H. H. Tan, and C. Jagadish, Selective area epitaxy of III–V nanostructure arrays and networks: Growth, applications, and future directions, Appl. Phys. Rev. **8**, 021302 (2021).

[3] J. Yoon, III-V nanomembranes for high performance, cost-competitive photovoltaics, MRS Adv. **2**, 1591 (2017).

[4] C.-Y. Chi, C.-C. Chang, S. Hu, T.-W. Yeh, S. B. Cronin, and P. D. Dapkus, Twin-free GaAs nanosheets by selective area growth: Implications for defect-free nanostructures, Nano Lett. **13**, 2506 (2013).

[5] G. Tutuncuoglu, M. de la Mata, D. Deiana, H. Potts, F. Matteini, J. Arbiol, and A. Fontcuberta i Morral, Towards defect-free 1-D GaAs/AlGaAs heterostructures based on GaAs nanomembranes, Nanoscale **7**, 19453 (2015).

[6] P. Aseev, A. Fursina, F. Boekhout, F. Krizek, J. E. Sestoft, F. Borsoi, S. Heedt, G. Wang, L. Binci, S. Martí-Sánchez *et al.*, Selectivity map for molecular beam epitaxy of advanced III-V quantum nanowire networks, Nano Lett. **19**, 218 (2019).

[7] M. Friedl, K. Cerveny, P. Weigele, G. Tütüncüoglu, S. Marti-Sanchez, C. Huang, T. Patlatiuk, H. Potts, Z. Sun, M. O. Hill *et al.*, Template-assisted scalable nanowire networks, Nano Lett. **18**, 2666 (2018).

[8] S. Conesa-Boj, E. Russo-Averchi, A. Dalmau-Mallorqui, J. Trevino, E. F. Pecora, C. Forestiere, A. Handin, M. Ek, L. Zweifel, L. R. Wallenberg *et al.*, Vertical "III–V" V-shaped nanomembranes epitaxially grown on a patterned Si[001] substrate and their enhanced light scattering, ACS Nano **6**, 10982 (2012).

[9] J. S. Lee, S. Choi, M. Pendharkar, D. J. Pennachio, B. Markman, M. Seas, S. Koelling, M. A. Verheijen, L. Casparis, K. D. Petersson *et al.*, Selective-area chemical beam epitaxy of in-plane InAs one-dimensional channels grown on InP(001), InP(111)B, and InP(011) surfaces, Phys. Rev. Mater. **3**, 084606 (2019).

[10] H. Schmid, M. Borg, K. Moselund, L. Gignac, C. M. Breslin, J. Bruley, D. Cutaia, and H. Riel, Template-assisted selective epitaxy of III–V nanoscale devices for co-planar heterogeneous integration with Si, Appl. Phys. Lett. **106**, 233101 (2015).

[11] J. Gooth, M. Borg, H. Schmid, V. Schaller, S. Wirths, K. Moselund, M. Luisier, S. Karg, and H. Riel, Ballistic one-dimensional InAs nanowire cross-junction interconnects, Nano Lett. **17**, 2596 (2017).

[12] J. Qu, D. V. Beznasyuk, M. Cassidy, R. Tanta, L. Yang, N. P. Holmes, M. J. Griffith, P. Krogstrup, and J. M. Cairney, Atomic-scale characterization of planar selective-area-grown InAs/InGaAs nanowires, ACS Appl. Mater. Interfaces **14**, 47981 (2022).

[13] A. Okamoto and K. Ohata, Selective epitaxial growth of gallium arsenide by molecular beam epitaxy, Appl. Phys. Lett. **51**, 1512 (1987).

[14] F. Allegretti, M. Inoue, and T. Nishinaga, *In-situ* observation of GaAs selective epitaxy on GaAs (111)B substrates, J. Cryst. Growth **146**, 354 (1995).

[15] P. Krogstrup, N. L. B. Ziino, W. Chang, S. M. Albrecht, M. H. Madsen, E. Johnson, J. Nygård, C. M. Marcus, and T. S. Jespersen, Epitaxy of semiconductor–superconductor nanowires, Nat. Mater. **14**, 400 (2015).

[16] R. S. Wagner and W. C. Ellis, Vapor-liquid-solid mechanism of single crystal growth, Appl. Phys. Lett. **4**, 89 (1964).

[17] M. Albani, L. Ghisalberti, R. Bergamaschini, M. Friedl, M. Salvalaglio, A. Voigt, F. Montalenti, G. Tütüncüoglu, A. Fontcuberta i Morral, and L. Miglio, Growth kinetics and morphological analysis of homoepitaxial GaAs fins by theory and experiment, Phys. Rev. Mater. **2**, 093404 (2018).

[18] M. Bollani, A. Fedorov, M. Albani, S. Bietti, R. Bergamaschini, F. Montalenti, A. Ballabio, L. Miglio, and S. Sanguinetti, Selective area epitaxy of GaAs/Ge/Si nanomembranes: A morphological study, Crystals **10**, 57 (2020).

[19] D. Dede, F. Glas, V. Piazza, N. Morgan, M. Friedl, L. Guniat, E. Nur Dayi, A. Balgarkashi, V. G. Dubrovski, and A. Fontcuberta i Morral, Selective area epitaxy of GaAs: The unintuitive role of feature size and pitch, Nanotechnology **33**, 485604 (2022).

[20] V. G. Dubrovskii, Criterion for selective area growth of III-V nanowires, Nanomaterials **12**, 3698 (2022).

[21] V. G. Dubrovskii and F. Glas, Vapor–liquid–solid growth of semiconductor nanowires, in *Fundamental Properties of Semiconductor Nanowires*, edited by N. Fukata and R. Rurali (Springer, Singapore, 2020).

[22] K. Tomioka, K. Ikejiri, T. Tanaka, J. Motohisa, S. Hara, K. Hiruma, and T. Fukui, Selective-area growth of III-V nanowires and their applications, Mater. Res. **26**, 2127 (2011).

[23] S. Hertenberger, D. Rudolph, M. Bichler, J. J. Finley, G. Abstreiter, and G. Koblmüller, Growth kinetics in position-controlled and catalyst-free InAs nanowire arrays on Si(111) grown by selective area molecular beam epitaxy, J. Appl. Phys. **108**, 114316 (2010).

[24] K. P. Bassett, P. K. Mohseni, and X. Li, Evolution of GaAs nanowire geometry in selective area epitaxy, Appl. Phys. Lett. **106**, 133102 (2015).

[25] M. E. Cachaza, A. W. Christensen, D. Beznasyuk, T. Særkjær, M. H. Madsen, R. Tanta, G. Nagda, S. Schuwalow, and P. Krogstrup, Selective area growth rates of III-V nanowires, Phys. Rev. Mater. **5**, 094601 (2021).

[26] F. Oehler, A. Cattoni, A. Scaccabarozzi, G. Patriarche, F. Glas, and J. C. Harmand, Measuring and modeling the growth dynamics of self-catalyzed GaP nanowire arrays, Nano Lett. **18**, 701 (2018).

[27] V. G. Dubrovskii, Theory of MBE growth of nanowires on reflecting substrates, Nanomaterials **12**, 253 (2022).

[28] V. G. Dubrovskii, Theory of MBE growth of nanowires on adsorbing substrates: The role of the shadowing effect on the diffusion transport, Nanomaterials **12**, 1064 (2022).

[29] W. Seifert, M. Borgstrom, K. Deppert, K. A. Dick, J. Johansson, M. W. Larsson, T. Martensson, N. Skold, C. P. T. Svensson, B. A. Wacaser *et al.*, Growth of one-dimensional nanostructures in MOVPE, J. Cryst. Growth **272**, 211 (2004).

[30] J. Johansson, C. P. T. Svensson, T. Martensson, L. Samuelson, and W. Seifert, Mass transport model for semiconductor nanowire growth, J. Phys. Chem. B **109**, 13567 (2005).

[31] V. G. Dubrovskii, G. E. Cirlin, I. P. Soshnikov, A. A. Tonkikh, N. V. Sibirev, Yu. B. Samsonenko, and V. M. Ustinov, Diffusion-induced growth of GaAs nanowhiskers: Theory and experiment, Phys. Rev. B **71**, 205325 (2005).

[32] M. C. Plante and R. R. LaPierre, Analytical description of the metal-assisted growth of III–V nanowires: Axial and radial growths, J. Appl. Phys. **105**, 114304 (2009).

[33] V. G. Dubrovskii, N. V. Sibirev, G. E. Cirlin, A. D. Bouravleuv, Yu. B. Samsonenko, D. L. Dheeraj, H. L. Zhou, C. Sartel, J. C. Harmand, G. Patriarche *et al.*, Role of non-linear effects in nanowire growth and crystal phase, Phys. Rev. B **80**, 205305 (2009).

[34] J. C. Harmand, F. Glas, and G. Patriarche, Growth kinetics of a single $InP_{1-x}As_x$ nanowire, Phys. Rev. B **81**, 235436 (2010).

[35] V. G. Dubrovskii and Yu. Yu. Hervieu, Diffusion-induced growth of nanowires: Generalized boundary conditions and

self-consistent kinetic equation, J. Cryst. Growth **401**, 431 (2014).

[36] P. Hanggi, P. Talkner, and M. Borkovec, Reaction-rate theory: Fifty years after Kramers, Rev. Mod. Phys. **62**, 251 (1990).

[37] F. Glas and V. G. Dubrovskii, Energetics and kinetics of monolayer formation in vapor-liquid-solid nanowire growth, Phys. Rev. Mater. **4**, 083401 (2020).

[38] G. E. Cirlin, V. G. Dubrovskii, N. V. Sibirev, I. P. Soshnikov, Yu. B. Samsonenko, A. A. Tonkikh, and V. M. Ustinov, The diffusion mechanism in the formation of GaAs and AlGaAs nanowhiskers during the process of molecular-beam epitaxy, Semiconductors **39**, 557 (2005).

[39] M. Borg, J. Johansson, K. Storm, and K. Deppert, Geometric model for metalorganic vapour phase epitaxy of dense nanowire arrays, J. Cryst. Growth **366**, 15 (2013).

[40] V. G. Dubrovskii, Y. Berdnikov, J. Schmidtbauer, M. Borg, K. Storm, K. Deppert, and J. Johansson, Length distributions of nanowires growing by surface diffusion, Cryst. Growth Des. **16**, 2167 (2016).